Journal of Materials Chemistry A

Accepted Manuscript

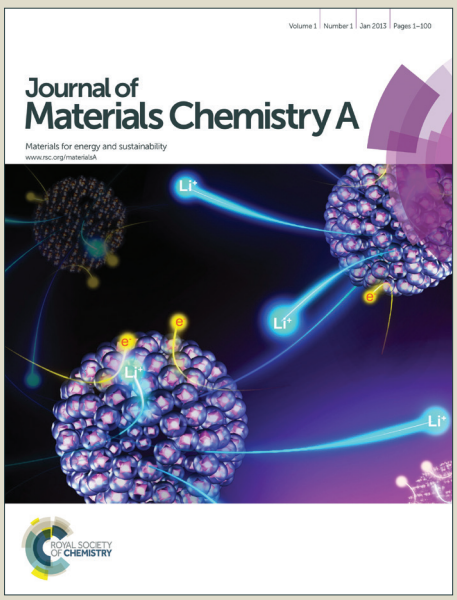

ROYAL SOCIETY OF CHEMISTRY

www.rsc.org/materialsA

ARTICLE

High performance composite polymer electrolyte using polymeric ionic liquid-functionalized graphene molecular brushes

Received 00th January 20xx,
Accepted 00th January 20xx

DOI: 10.1039/x0xx00000x

www.rsc.org/

Yun-Sheng Ye,[a*] Hao Wang,[a] Shu-Guang Bi,[a] Yang Xue,[a] Zhi-Gang Xue,[a] Xing-Ping Zhou,[a] Xiao-Lin Xie,[a*] and Yiu-Wing Mai[b]

A new structural design and tailored morphology of polymer-functionalized graphene (polymer-FG) is employed to optimize composite polymer electrolytes (CPEs). The ionic transfer conditions including Li salt dissociation, amorphous content and segmental mobility are significantly improved by incorporating polymer-FG, especially that having a polymeric ionic liquid (PIL) and a polymer brush structure [PIL(TFSI)-FG_{brush}]. Electrical shorts are eliminated due to the presence of the functionalized polymer on reduced graphene oxide (RGO) and a minimal amount of polymer-FG in the PEO/Li^+ polymer electrolytes (PEs). Polymer-FG with PIL brushes increases significantly the Li ion conductivity of PEO/Li^+ PE by >2 orders of magnitude and ~20-fold at 30 °C and 60 °C with high Li salt loading (O/Li= 8/1), respectively. Furthermore, significant improvements in mechanical properties are observed where only 0.6 wt% addition of the PIL(TFSI)-FG_{brush} led to more than 300% increase in the tensile strength of the PEO/Li^+ at an O/Li ratio of 16/1. Li-ion battery performance was evaluated with the CPE containing 0.6 wt% of PIL(TFSI)-FG_{brush}, resulting in superior capacity and cycle performance compared to that of the PEO/Li^+ PE. Thus, we believe by embedding minimal amounts of structurally and morphologically optimized polymer-FG nano-fillers, it can lead to the development of a new class of SPEs with high ionic conductivity for high performance all-solid-state Li-ion batteries.

Introduction

Solid polymer electrolytes (SPEs) provide advantages such as improved mechanical strength, formability, lack of solvent leakage, decreased dendritic growth, and reduced interfacial reactions, when compared to electrolytes based on solvents or gels in lithium metal or lithium ion batteries.[1, 2] Despite their advantages on stability and battery safety, application of SPEs has been limited by their low conductivity. A SPE, formed by the dissolution of a lithium salt (LiX) in a poly(ethyl oxide) (PEO) matrix, in which Li^+ ions coordinate with the oxygen groups of ethers, has been widely investigated.[3, 4] Although PEO, when used as a matrix in polymer electrolytes (PEs), has advantages such as chemical and electrochemical stability and ability to solvate a variety of alkali metal salts, its low ionic conductivity at room temperature (≤10^{-6} S/cm) has compromised the lithium ion battery performance.[5, 6] To overcome this problem, several techniques have been attempted such as increasing the amount of lithium salt, adding low-molecular-weight plasticizers, and incorporating nano-fillers into the polymer matrix.[6-11] The first two approaches have been successful in increasing the ion conductivity, but have also led to compromises in the mechanical properties because the plasticized polymer chains are relatively flexible, hence decreasing the mechanical stability and strength. The third approach by addition of nano-fillers, however, not only improves the ion conductivity and interfacial stability of the polymer electrolyte (in contact with metallic lithium), but also its mechanical reliability and strength.[12] Nonetheless, further work is still needed to optimize the structure of the composite polymer electrolytes (CPEs) by tailoring the morphology of the nano-fillers.

Researchers have reported that incorporation of nano-scale ceramic fillers (SiO_2, Al_2O_3, TiO_2, and ZrO_2)[13-16] and clays[17-19] into PEs improves both the ionic conductivity and the mechanical strength and stability. Carbon nanotubes (CNTs), used as nano-fillers in CPEs, have also been seen as potential candidate materials offering the potential to enhance properties of strength, modulus, thermal stability and high aspect ratio. The strong affinity between the CNT's rich electron cloud and the Li^+ ions facilitates Li salt dissociation and ion transport through the PE.[20, 21] Graphene oxide (GO) have been used as fillers in fuel cell polymer membrane applications and have led to significant improvements in ionic conductivities, mechanical properties and power densities.[22-25] GO has also been introduced into PEO/Li^+ PE for Li-ion battery applications and showed a significant improvement in ionic conductivity (nearly two orders) and a 260% increase in the tensile strength of the SPE with 1 wt% GO content.[26] Moreover, it has been reported that the ionic conductivity of SPE can be effectively improved (one order of magnitude higher than pristine SPE) by introducing only 0.2 wt% poly(ethylene glycol)-functionalized-GO (PEG-FGO), because a larger amount of Li salt can be dissociated in the CPE by Lewis acid-base interactions between PEG and Li salt.[27] Although GO/graphene-based nano-fillers can improve both ionic conductivities and mechanical properties, however, the effects of their structure design and tailoring on the SPE for Li-ion battery application have not been explored yet.

[a] *Address here. Key Laboratory for Large-Format Battery Materials and Systems, Ministry of Education, School of Chemistry and Chemical Engineering, Huazhong University of Science and Technology, Wuhan 430074, China.*
[b] *Centre for Advanced Materials Technology (CAMT), School of Aerospace, Mechanical and Mechatronic Engineering J07, The University of Sydney, Sydney NSW 2006, Australia*

† Electronic Supplementary Information (ESI) available: [details of any supplementary information available should be included here]. See DOI: 10.1039/x0xx00000x

Successful preparation of CPEs depends on the dispersion of nano-fillers in polymer matrix, since it correlates directly with improvements in impermeability, and resulting mechanical and electrical properties.[28] Optimized surface modifications, prior to incorporation into CPEs, improve the compatibility of nano-fillers with the polymer matrix by forming homogeneous dispersions. Functionalization with polymeric chains is one of most efficient method to improve the dispersion of nano-fillers in the polymer matrix and enhance the nano-filler/matrix interaction.[29, 30] Moreover, it has been reported that the Li ions can potentially find low-energy conducting pathways along the nano-filler/matrix interface.[21, 31] Hence, CPEs incorporated with highly-dispersed polymer-functionalized nano-fillers facilitate forming continuous inter-connected ion conducting channels, which reduce the ion traveling resistance during the slow segmental motions of the polymer chains.[22] In addition, the dissolvability of Li salt can be enhanced by introducing the interactions between the grafted polymer of nano-fillers and Li salt, which is favorable to the transfer of Li-ions.[4, 27, 32]

Recently, GO/graphene-based two-dimensional (2D) molecular brushes with various types of polymers have been prepared and their high solubility, low viscosity and good processability make them promising in many applications.[33] Polymeric ionic liquids (PILs) are also finding applications in many different technology fields; one of which is used as ion conducting SPEs in electrochemical devices because of the combination of unique properties of ILs with macromolecular architecture.[34, 35] Herein, we have prepared reduced GO-based 2D molecular brushes with PIL arms [PIL(TFSI)-FG_{brush}], and they were applied as the nano-filler material to optimize the ionic transfer conditions of the PEO/Li^+ PEs. For comparison, PEG-functionalized RGO molecular brushes (PEG-FG_{brush}) and PIL-functionalized RGO [PIL(TFSI)-FG] were also prepared and introduced into PEO/Li^+ PEs to show the effects of structure design and tailoring of graphene-based nano-fillers on the SPE for Li-ion battery application. Importantly, the ionic transfer conditions, such as dissociation of Li salt, amorphous content, and segmental mobility in CPEs, were improved by adding polymer-functionalized RGO (polymer-FG). Thus, the polymer-FG having a PIL and a polymer brush structure in CPEs is found to be the critical structural design to improve the ionic conductivity, mechanical properties and performance of SPE Li-ion batteries. For the first time we have prepared polymer-FG having a PIL and a polymer brush structure for a new class of SPEs with high ionic conductivity for high performance all-solid-state Li-ion batteries.

Experimental

Chemicals and Materials

GO was prepared using a modification of Hummers and Offeman's method according to our previous study.[22] Alkyne-functionalized RGO (Alkyne-FG), azido-terminated poly (ethylene glycol) (PEG-N_3), and azido-terminated poly(2-dimethylamino ethyl methacrylate) (PDMA-N_3) were synthesized according to a previously published report.[36, 37] 2-dimethylamino ethyl methacrylate) (DMA, 98 % from Sigma-Aldrich), 1,8-diazabicyclo[5.4.0]undec-7-ene (DBU, 98% from Aldrich), copper(I) iodide [Cu (I), 98% from Sigma-Aldrich], lithium perchlorate ($LiClO_4$, ≥99.0% from Sigma-Aldrich), lithium bis(trifluoromethanesulfonyl)Imide (LiTFSI, ≥99.0% from Sigma-Aldrich), and PEO (M_n ~600,000 g mol^{-1} from Acros) were used as-received.

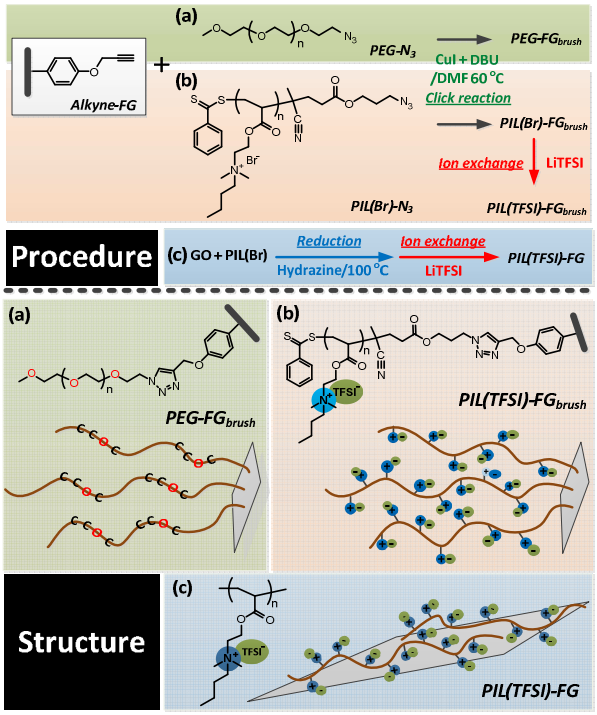

Scheme 1. Schematic diagram for the synthesis of of polymer-functionalized RGO brush (Polymer-FG_{brush}) and PIL(TFSI)-FG.

Synthesis and Preparation of Polymer-functionalized Graphene Brush (polymer-FG_{brush}) [Scheme 1 (a) and (b)]

The azido-terminated polymeric ionic liquid [PIL(Br)-N_3] was prepared by reacting PDMA-N_3 with 1-bromobutane in methanol at 30 ˚C for 24 h followed by precipitation in ethyl acetate (EA) to obtain the final product. In a typical experiment, a 50 mL flask was charged with alkyne-FG (50 mg) and DMF (10 mL). Sonication for 0.5 h at room temperature resulted in the formation of a black suspension, to which PEG-N_3 or PIL(Br)-N_3 (0.2 g), Cu (I) (0.16 g, 0.83 mmol) and DBU (6.31 g, 41.5 mmol) were added. The reaction mixture was evacuated and refilled with nitrogen three times, followed by stirring under argon at 60 °C for 24 h. Then, the mixture was diluted with 200 mL THF, bath-sonicated for 10 minutes, and filtered through a 200 nm PTFE membrane. The resulting black solid was washed thoroughly with THF (5×50 mL), methanol, water, and methanol, and then dried under vacuum overnight. Following our previous studies,[22] PIL(TFSI)-FG_{brush} was prepared by ion exchange with lithium bis(tri-fluoromethyl-sulfonyl) amide (LITFSI) to replace the Br anion with the TFSI anion of the PIL on the RGO surface.

Synthesis and Preparation of Polymeric Ionic Liquid-functionalized Graphene [PIL(TFSI)-FG] [Scheme 1 (c)]

The polymeric ionic liquid, PIL(Br), poly(2-dimethylamino ethyl methacrylate) bromide, was synthesized according to a previously reported procedure.[38] To prepare the PIL(Br)-FG, 2 mmol of PIL(Br) were dissolved in water and added to 20 mL (1.5 mg mL^{-1}) of an aqueous GO suspension. The mixture was then reduced with hydrazine (3.5 mmol) at 90 ˚C for 2 h under continuous stirring. After reduction, a dispersion of PIL(Br)-FG was centrifuged several times to remove residual PIL(Br) and then re-dispersed in water under sonication. PIL(TFSI)-FG was prepared by ion exchange with LITFSI to obtain PIL(TFSI)-FG.

Preparation of PEO/Li^+ and PEO/Li^+/polymer-FG CPEs

PEO was dissolved in CH_3CN (with 10 wt% solid content) and stirred at 30 °C for 3 h. A solution comprising different ratios of Li salt ($LiClO_4$), PEO and polymer-FG was stirred and ultra-sonicated in acetonitrile (CH_3CN) to obtain a homogeneous solution, which was then added to the PEO/CH_3CN solution and stirred at 30 °C overnight. The PEO/Li^+ or PEO/Li^+/polymer-FG solution was cast onto a Teflon mold and dried at 60 °C for at least 24 h and then heated at 80 °C to remove any residual solvent.

Characterization

The ionic conductivity of the membrane was determined with an electrochemical impedance analyzer (PGSTAT 30). The experiments involved scanning the ac frequency, from 100 kHz to 10 Hz, at a voltage of 10 mV. The electrical conductivity of PEO/polymer-FG composites was measured using a standard four-probe method. The morphology of the polymer-FG in the composites was observed using a JEOL JEM-1200CX-II transmission electron microscope operated at 120 kV. Scanning electron microscopy (SEM) images were taken with a Hitachi S-4700 microscope using an accelerating voltage of 15 kV.

FTIR spectra were obtained with a Nicolet Avatar 320 FTIR spectrometer; 32 scans were collected at a spectral resolution of 1 cm^{-1}. The samples for FTIR measurement were prepared by solution deposition on salt plates. XPS measurements were made [ESCA 2000 (VG Microtech)] using a monochromatized Al Kα anode. The internal solvent peak was used to calibrate the chemical shift in the NMR data. A HITACHI L-7100 pump, a RI 2000 refractive index detector (Schambeck SFD GmbH) with an elution rate of 1.0 mL min^{-1}, at a temperature of 80 °C, with a Polymer Laboratories PLgel guard column (5 µm particles; 50×7.5 mm^2) and a PLgel 5 µm mixed-D column (300×7.5 mm^2; particle size 5 µm,) were connected in series. The molecular weight calibration curve was obtained using PEO standards of defined molecular weight (1010-163000 g mol^{-1}) (Polymer Laboratories Inc., MA). The thermal degradation behavior of the membranes was measured using a Q50 thermo-gravimetric analyzer (TGA), operated from room temperature to 850 °C, at a heating rate of 10 °C min^{-1}, in a nitrogen atmosphere. The glass transition temperature (T_g) was measured using a DuPont TA Instrument Q20 differential scanning calorimeter (DSC) from -90 to 100 °C at a heating rate of 5 °C min^{-1} in a nitrogen atmosphere. X-ray diffraction (XRD) analyses were performed on a Bruker D8 Advance diffractometer with Cu-Kα radiation. The diffraction data were recorded for 2Θ angles from 10° to 50°. The tensile properties were measured according to ASTM D882 on a Shimadzu AG-50 kN universal tester. The crosshead speed was set at 5 mm min^{-1}. The electrical conductivity of the PEO filled with polymer-FG without Li salt was also measured using a standard four-probe method.

Electrochemical measurements

The Li transference number (t_{Li^+}) was determined using a method combining dc polarization and ac impedance measurements, proposed by Evans et al.[39] The current and resistance were measured using a PGSTAT 30 impedance analyzer. The sample was sandwiched between two 0.5 mm-Li foils (Alfa) as non-blocking electrodes and assembled in a standard 2032 coin-cell holder in an argon gas filled glove box. Finally, it was placed into an outside oven: 10 mV was then applied to the cell and the current was monitored as a function of time until the steady state was achieved.

A Li/$LiFePO_4$ coin cell was used to evaluate the performance of the CPEs in Li battery applications. Li foil (battery grade) was used as the negative electrode. The thickness and surface area of the Li foil were 0.5 mm and 1.54 cm^2, respectively. The positive electrode was fabricated by spreading a mixture of $LiFePO_4$, acetylene black and PEO-$LiClO_4$ complex (Li ion conductor and binder; initially dissolved in CH_3CN) with a weight ratio of 8.0:0.5:1.5 onto an Al current collector (battery use). Loading of active material was about 2.0~2.5 mg cm^{-2}: this thinner electrode was directly used without pressing. Cell construction was conducted in the glove box, and all the cell components were dried in vacuum before being placed into the glove box. Cell performance was examined by a galvano-static charge - discharge cycling test using a CT2001A cell test instrument (LAND Electronic Co., Ltd.) and a computer-controlled battery tester between 3.0 and 4.2 V at 60 °C at a current density of 0.1 C. Before the electrochemical measurements, all the assemble chamber at the cell operation temperature (60 °C) for 12 h to enhance adhesion at the Li/SPE and SPE/$LiFePO_4$ interfaces.

Results and discussion

Synthesis and Characterization of Polymer Functionalized-Reduced Graphene Oxide Molecular Brush

Following our previous studies, non-covalent PIL(TFSI)-FG was prepared by the reduction of PIL(Br) and GO mixing solution, followed by ion exchange with LiTFSI to replace Br anion with TFSI anion of PIL on RGO surface.[22] Covalent PEG-FG_{brush} were obtained from alkyne-functionalized RGO (alkyne-FG) using the 'grafting to' strategies in combination with reversible chain transfer and click chemistry.[36] PIL(TFSI)-FG_{brush} was prepared using the same approach and was followed by ion exchange to obtain the final product (see experimental section).[22] The quality and grafting density of PEG-FG_{brush} and PIL(TFSI)-FG_{brush} were characterized by TGA, FTIR spectroscopy, XPS and TEM.

To understand the influences of different types of RGO surface polymer brushes on ionic transfer by PEO/Li^+ polymer electrolytes, the chain length of the grafted polymer and the grafting density of the resulting polymer-FG must be considered; these being crucial factors for RGO dispersion and interface properties. According to our previous study,[36, 37] the use of the 'grafting to' approach allows full control over the limited length of grafted polymer chains, while permitting a high grafting density to a single RGO surface, hence resulting in good solubility and processability. Thus, the 'grafting to' approach was used to prepare polymer-FG in this study whose grafting densities are shown in **Table 1**. Clearly, both polymer-FG molecular brushes formed by the 'grafting to' approach show similar grafting ratio and grafting density, indicating that structural differences do not affect the grafting reaction and that the polymer brush chain length and grafting density are well controlled.

Table 1. Molecular weight and grafting density of alkyne-FG and polymer-FG.

Sample	M_n[a] (g mol^{-1})	Grafting ratio (wt%)[b]	$\bar{A}_{pg1}$[c] (chains per 10^5 carbons)	$\bar{A}_{pg2}$[d] (chains μm^{-2})
Alkyne-FG	131	34.2	24.7	4.67×10^5
PEG-FG_{brush}	5025 PEG-N_3	58.2	20.9	4.00×10^4
PIL(Br)-FG_{brush}	6290 PIL(Br)-N_3	59.9	18.6	3.55×10^4
PIL(Br)-FG	13000 PIL(Br)	60.2	-	-

[a] Determined by GPC measurements at root temperature in which THF was used as an eluent and PS standard for calibration.

[b] Determined from weight loss at 800 °C.

[c] Calculated from eq S1.

[d] Calculated from eq S2.

Figure 1 shows the FTIR spectra for alkyne-FG and polymer-FG molecular brushes. The absorbance peaks of alkyne-FG at 1108, 1614, 1740, 2125, and 3282 cm^{-1} can be attributed to C-O stretching, C=C in carboxylic moieties, C=O assigned to skeletal vibrations of un-oxidized graphite domains, C≡C stretching, and C-H stretch of C-H bond adjacent to the carbon-carbon triple bond, respectively. After the grafting reaction, two new peaks at 1171 and 1338 cm^{-1}, corresponding to C-O stretching and the TFSI anion, appear in spectrum (b) of PEG-FG_{brush} and (c) of PIL(TFSI)-FG_{brush}, due to the PEG and PIL(TFSI), respectively, present in the products. XPS C1s core-level spectra of alkyne-FG, PEG-FG_{brush} and PIL(TFSI)-FG_{brush} are shown in **Figure 2**. The XPS C1s core-level spectrum of alkyne-FG can be resolved by curve-fitting into four peak components with binding energies of ~284.5, 285.6, 285.9, and 286.5 eV, attributable to sp^2 hybridized C-C in the aromatic ring, sp^3 hybridized carbon, and C=N and C-O species, respectively.[22] After the grafting reaction, C1s core-level spectra of PEG-FG_{brush} and PIL(TFSI)-FG_{brush} show a marked increase in the intensity of the sp^3 hybridized carbon (285.6 eV) and the C-O (286.5 eV) peak component. Several peak components appear in the PIL(TFSI)-FG_{brush} spectrum; for example, peaks at 287.0 eV and 288.5 eV represent C-F and C=O, respectively. Broad signals at 169.1 eV in the S2p region and 689.3 eV in the F1s region corresponding to the TFSI anion appear, indicating that the Br anion of PIL has been successfully replaced by the TFSI anion.

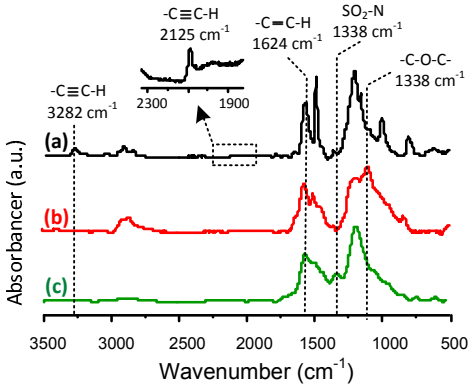

Figure 1. Fourier transform infrared (FTIR) spectra of: (a) alkyne-FG, (b) PEG-FG_{brush}, and (c) PIL(TFSI)-FG_{brush}.

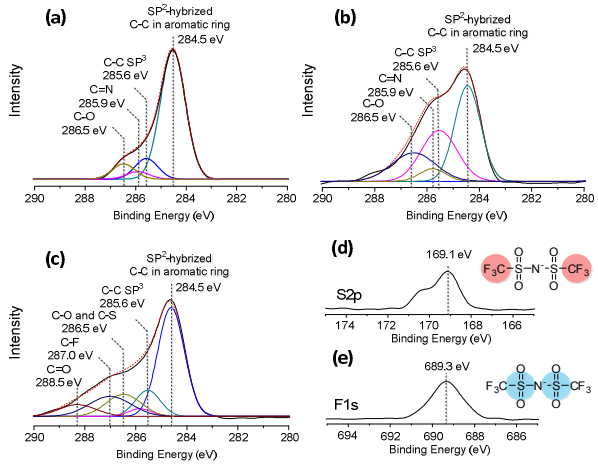

Figure 2. C1s XPS profile of (a) alkyne-FG, (b) PEG-FG_{brush}, (c) PIL(TFSI)-FG_{brush}; and (d) S2p XPS and (e) F1s of PIL(TFSI)-FG_{brush}.

The dispersibility and compatibility of polymer-FG sheets impact strongly the physical properties of the SPE. To evaluate the dispersibility of the polymer-FG species in different solvents, approximately 1.5 mg of polymer-FG powder was added to a given volume of solvent (~1.5 mL), so that the resulting nominal concentration was adjusted to 1 mg mL^{-1} in all cases. The results are shown in **Figure 3**. It is clear that the solubility of the polymer-FGs is strongly dependent on the nature of the grafted polymer (**Figure S1**); for example, the solubility is largely consistent with that of the original polymer in un-grafted state. Before introducing the polymer-FGs into PEO/L^{i+} PE, we tested the solubility of the polymer-FGs in CH_3CN, which was chosen as the mixing solvent to prepare PEs in this study. A sample of each polymer-FG (~100 mg) was

dispersed in 20 mL of CH_3CN and allowed to stand over-night to enable any insoluble material to settle. The supernatant from this solution was dried and the resulting solubility values were determined as 212, 144, and 173 mg L^{-1} for PIL(TFSI)-FG, PEG-FG_{brush}, and PIL(TFSI)-FG_{brush}, respectively. The difference in solubility of the polymer-FGs may be attributed to the nature of the grafted polymer and modification method. TEM was used to determine if graphene-based sheets existed in the solvent as single exfoliated sheets, or as multi-layered platelets. As shown in **Figure S2**, TEM image shows that all three polymer-FGs are fully exfoliated into individual sheets in CH_3CN. These results indicate that polymer modification is an effective approach for improving the solubility of the RGO sheets in organic solvents and favors the formation of homogeneous dispersions in polymer matrices by solvent blending.

The resulting PEO/Li^+/PIL(TFSI)-FG_{brush} CPE containing 0.6 wt% of PIL-FG_{brush} [see top left inset in **Figure 4(a)**] is semi-transparent and freestanding. Its fracture surface after UV etching is shown in **Figure 4(a)**. The original PEO/Li^+/PIL(TFSI)-FG_{brush} CPE exhibits a wrinkled surface morphology. But, with UV light etching, sheet morphologies are revealed (e.g., by dotted chains) and randomly dispersed as a 3D network throughout the PEO/Li^+ PE. Also, **Figure 4(b)** shows the TEM image of the PEO/Li^+/PIL(TFSI)-FG_{brush} CPE displaying randomly dispersed graphene sheets. The homogeneous dispersion of PIL-FG_{brush} is due to the PIL which has enhanced the interfacial compatibility with Li salt and PEO matrix.

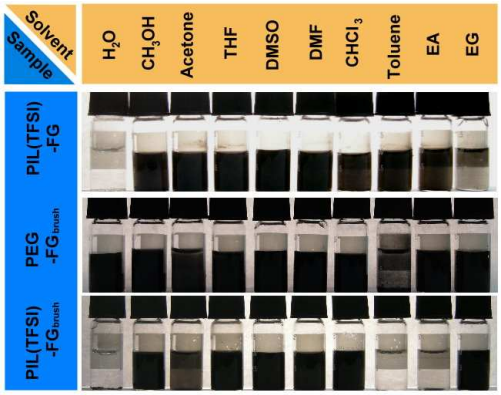

Figure 3. Photographs of polymer-FGs in various solvents.

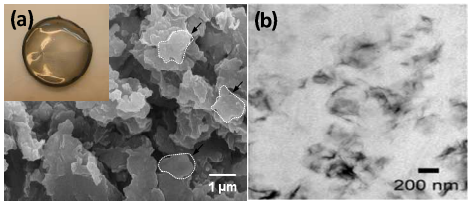

Figure 4. (a) SEM image and (b) TEM image of PEO/Li^+/PIL(TFSI)-FG_{brush} 0.6 wt% CPE.

Thermal Properties of PEO/Li^+ and PEO/Li^+/polymer-FG CPE

The ionic conductivity of SPEs is viewed as being confined to the amorphous phase above the glass transition temperature, T_g, where the polymer chain motion creates a dynamic, disordered environment that plays a critical role in facilitating ion transport. Generally, the lower the T_g values, the higher the mobility of the SPE. Thus, a decrease in T_g helps easy movement of the polymer chains, which results in an increase in conductivity. **Figure S3** shows the thermal properties of the PEO/Li^+ and PEO/Li^+/polymer-FG CPEs. The addition of PIL(TFSI)-FG shows a limited effect on T_g, however, decrease in T_g is observed when adding both polymer-functionalized RGO brushes (polymer-FG_{brush}) in PEO/Li^+ PE, especially in the PEO/Li^+/PIL(TFSI)-FG_{brush} CPE. These results indicated that the T_g values of the PEO/Li^+/polymer-FG CPE are more strongly affected by the presence of polymer brushes; that is, the decrease of segmental mobility in the incorporated polymer-FG_{brush} CPE is larger than by introducing polymer-FG without polymer brushes in PEO/Li^+ PE at a given salt concentration. We can conclude that polymer-FG with molecular brush structure strengthens the interaction of multi-functional groups of polymer brushes with PEO matrix or Li salt; thereby weakening the interaction of PEO matrix with Li salt and decreasing the T_g of the PEO/Li^+ PE. Similar behavior was reported for polymer-functionalized CNT and polymer-FGO composites.[27, 40]

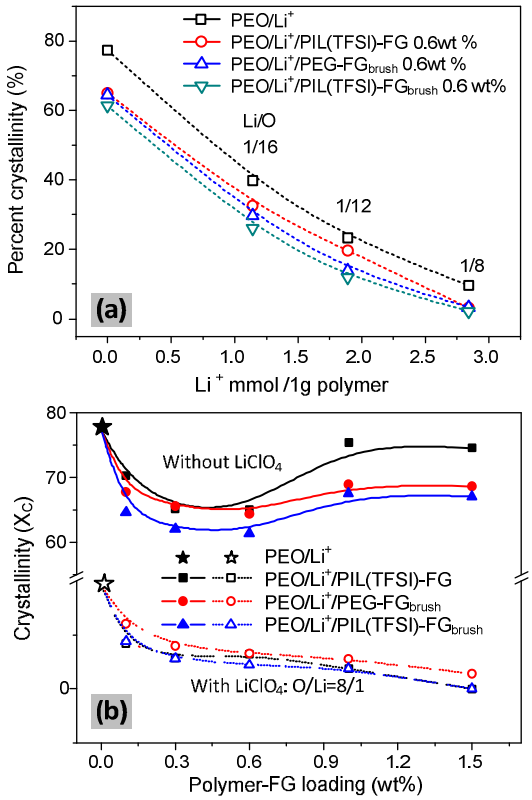

Figure 5. (a) Percent crystallinity *versus* Li^+ ion concentration. (b) Percent crystallinity *versus* polymer-FG loading.

The degree of crystallinity of PEO/Li^+ PE and PEO/Li^+/polymer-FG CPE is determined by using DSC and XRD. **Figures 5(a)** and **5(b)** show the crystallinity of PEO/Li^+ PE and PEO/Li^+/polymer-FG CPEs with various polymer-FG loading (from 0.3 to 1.5 wt%) and salt concentration (O/Li= 16/1, 12/1, 8/1). The percentage of crystalline PEO, X_c, can be calculated from: $X_c = (\Delta H_m/\Delta H^0_m) \times 100\%$, where ΔH_m is the fusion heat of PEO/Li^+/polymer-FG CPEs (calculated from the integral area of the DSC curves), and ΔH^0_m is melting enthalpy of a completely crystalline PEO sample, 213.7 J g^{-1} (100% crystalline).[4] By adding $LiClO_4$, the crystallinity of PEO is reduced significantly with increasing salt concentration and is almost completely amorphous at salt concentrations up to O/Li= 8/1 [**Figure 5(a)**]. It is suggested that the interaction of PEO···Li^+ destroys the regular crystallinity and reduces the degree of crystallinity of the PEO. Figure 5(b) shows that X_c is strongly influenced by polymer-FG loading. By adding polymer-FG sheets into the PEO matrix (see solid symbols), X_c first drops (reaching a minimum at 0.6 wt% polymer-FG loading) and then rises. This result shows that randomly dispersed polymer-FG facilitates suppression of PEO crystallization and more so for the PEO/Li^+ PE containing polymer-FG (see unfilled symbols in **Figure 5(b)** where X_c of PEO in the CPEs decreases from 10% to 1% as polymer-FG loading increases to 1.5 wt%), which is similar to incorporated GO in PEO/Li^+ CPE.[26] However, the reduction in crystallinity of PEO or PEO/Li^+ is more obvious by introducing the PIL(TFSI)-FG_{brush}.

The crystallization behavior of PEO and PEO/PIL(TFSI)-FG_{brush} are further investigated by using XRD measurement. The XRD pattern (**Figure S4**) of pure PEO without Li salt has many dominant peaks in the range 2Θ~ 19° and 23°, indicating semi-crystalline nature of the polymer.[41] An increase in salt concentration in PEO/Li^+/polymer-FG CPE causes the intensity of these peaks to decrease more obviously as compared to the PEO/Li^+ PE, which is also consistent with the DSC result. We speculate that the additional complexation of the cation of PIL brushes in PEO matrix can further suppress the PEO crystallization. Therefore, the introduction of PIL(TFSI)-FG_{brush} in the PEO/Li^+ PE provides additional conducting ions. And it also reduces T_g and X_c, which increases the flexibility of the PEO chains and the ratio of amorphous PEO, respectively. As a result, the ionic conductivity should be enhanced at lower temperatures.

Influence of Polymer-FG on Ion Pairing of PEO/Li^+ PE

The FTIR spectra were used to study the ion-ion interactions between PEO, Li salt ($LiClO_4$) and polymer-FG. The ClO_4^- in PEO generally shows two bands in the spectra:[3, 4] one band centered at 625 cm^{-1} has been assigned to the vibration of the "free'' ClO_4^- anion, which does not interact directly with the Li cations, and the other one centered at 635 cm^{-1} is due to the vibration of the Li^+ and ClO_4^- contact-ion pairs. The fraction of "free'' ions and ion pairs can be calculated by integrating the area under the two peaks. The spectroscopically "free'' ions are believed to be responsible for ionic charge transport in the PEs. Hence, the fraction of free'' ions will indicate the effectiveness of different PE/polymer-FGs in increasing charge concentration and subsequent ion conduction.

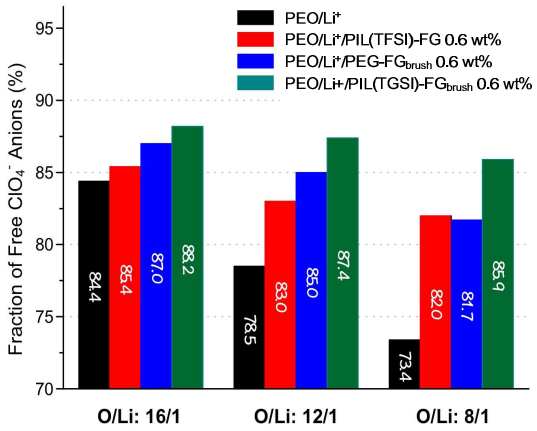

Figure 6. Fraction of dissociated salt ions (ClO_4^- anions) based on FTIR analysis of pure PEO/Li^+ and PEO/Li^+/polymer-FG CPEs.

The fractions of "free'' anions as a function of salt concentration for PEO/Li^+ and PEO/Li^+/polymer-FG CPEs are shown in **Figure 6**. The dissociated Li salt ions in all PEs are increased by increasing the salt concentration (O/Li: from 16/1 to 8/1). This is expected since more and more free ions become bound with the opposite ions to form contact ions upon addition of more salt. The incorporation of all polymer-FG shows a limited effect on the dissociation of Li salt at low salt concentration (O/Li= 16/1). However, with higher Li salt loading (O/Li= 8/1), adding polymer-FG into PEO/Li^+ PE can result in an increase of free ions (from 73.4% to 82.0% and 81.7% for PEO/Li^+/PIL(TFSI)-FG 0.6 wt% and PEO/Li^+/PEO-FG_{brush} 0.6 wt%, respectively) and a maximum of 85.9% is reached as RGO is modified with the PIL molecular brush. This suggests that the polymer-FG sheets can effectively facilitate the dissociation of Li salt by weakening the interaction between contact-ion pairs, resulting in the increased charge carrier concentration. Specifically, when polymer-FG with a PIL structure and a polymer brush morphology is more effective to enhance the dissolvability of Li salt and release more free ions, which are favorable to the transfer of Li-ions.

Ionic Conductivity of PEO/Li^+ and PEO/Li^+/Polymer-FG CPEs

The ionic conductivity $\sigma(T)$ of PE depends on the effective number of charge carriers (n_i), ionic charge (q_i), and the ions mobility (μ_i), according to: [42]

$$\sigma(\mathrm{T}) = \sum_i n_i q_i \mu_i$$

The effective number of charge carriers is related to the concentration of the dissolved ions. The ion mobility in a PE, formed by the dissolution of ions in the polymer, is facilitated by the segment mobility of the polymer chains. By incorporating polymer-FG sheets into the PEO/Li^+ PE, it may act differently depending on the filler loading, surface

modification, grafting polymer structure and distribution. **Figure 7** shows the percent crystallinity of PEO/Li^+ and PEO/Li^+/polymer-FG CPEs as a function of dissociated Li^+ ion concentration. The addition of the polymer-FG sheets in PEO/Li^+ PE shows a cooperative effect on the dissociation of Li salt and suppression of the PEO crystallization. Among these polymer-FGs, the most effective is the PIL(TFSI)-FG_{brush}, which has the highest amorphous content and dissociated Li^+ ion concentration at all salt concentrations. Also, the higher segmental mobility in PEO/Li^+/PIL(TFSI)-FG_{brush} CPE, as revealed by DSC, is strengthened by the higher amounts of charge carriers. This property confers upon PEO/Li^+/PIL(TFSI)-FG_{brush} CPE the best ionic transfer conduction of all PEO/Li^+/ polymer-FG composite systems.

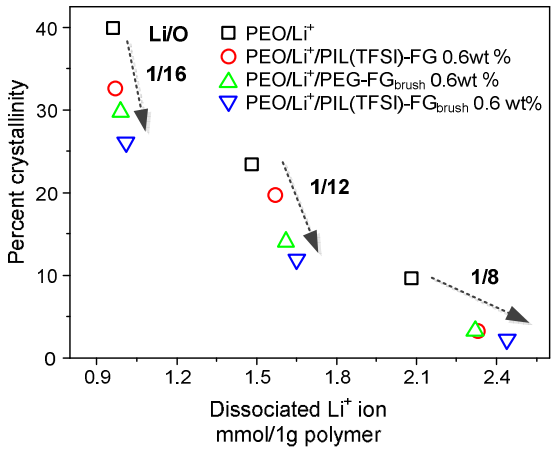

Figure 7. Percent crystallinity *versus* dissociated Li^+ ion concentration.

Before the ionic conductivity measurement, we performed four-point probe resistivity measurement of PEO filled with PIL(TFSI)-FG (1.5 wt%) without Li salt and found the electrical conductivity value below 10^{-7} S cm^{-1} at 30 ˚C. This result indicated that the electron condition in CPEs was well controlled and the risk of electrical shorts was eliminated. **Figure S5** and **Figure 8(a)** shows the ionic conductivity of PEO/Li^+ PEs with various polymer-FG contents at 30 ˚C and 60 ˚C, respectively with high salt loading (O/Li= 8/1). The ionic conductivity of the PEO/Li^+ PEs is not varying significantly with respect to polymer-FG content, and the maximum conductivity (7.9×10^{-5} S cm^{-1} at 30 ˚C; 1.5×10^{-4} S cm^{-1} at 60 ˚C) is reached at a 0.6 wt% PIL(TFSI)-FG_{brush} loading. Significantly, the combined (1) amorphous content, (2) salt dissociation and (3) ion mobility enhancements appear to be effective in giving overall increases of >2 orders of magnitude and ~20-fold in ion conductivity at 30 ˚C and 60 ˚C (ion conductivity of PEO/Li^+ PE: 0.7×10^{-6} S cm^{-1} at 30 ˚C and 7.8×10^{-5} S cm^{-1} at 60 ˚C), respectively. Moreover, the exfoliated polymer-FG sheets in the PEO/Li^+ PE have the ability to facilitate ion transport on their external surfaces and form 3D ion transport channels throughout the PEs. With further increase in the polymer-FG content (>0.6 wt%), the ionic conductivity decreases slightly, indicating potential polymer-FG aggregation and orientation in the plane of PE that impedes Li ion through-plane transport in PEO matrix.[31]

In general, the ionic conductivity increases with increasing salt concentration as the total number of charge carriers increases. However, when the salt concentration increases in the PE, formation of associated ionic species also increases, which reduces the overall mobility and the number of effective charge carriers. Hence, only slight increases in ionic conductivity are observed with increased $LiClO_4$ doping in pure PEO/Li^+ PE [**Figure 8(b)**]. However, addition of polymer-FGs in PEO/Li^+ PE significantly increases the ionic conductivity with increasing salt concentration and reaches maximum value at an O/Li ratio of 8/1. Among the polymer-FGs, PIL(TFSI)-FG_{brush} gives the highest increase in ionic conductivity by at least one order of magnitude compared to pure PEO/Li^+ PE at all salt contents. The ionic conductivity of the CPEs has also been examined at various temperatures (30-80 ˚C) and polymer-FG loadings with a fixed salt an O/Li ratio of 8/1. It can be seen from **Figure S5** that the ionic conductivity is significantly enhanced by the addition of PIL(TFSI)-FG_{brush} (0.6 wt%) in PEO/Li^+ PE, reaching values of 7.8×10^{-5} S cm^{-1} at 30 ˚C and 4.0×10^{-4} S cm^{-1} at 80 ˚C.

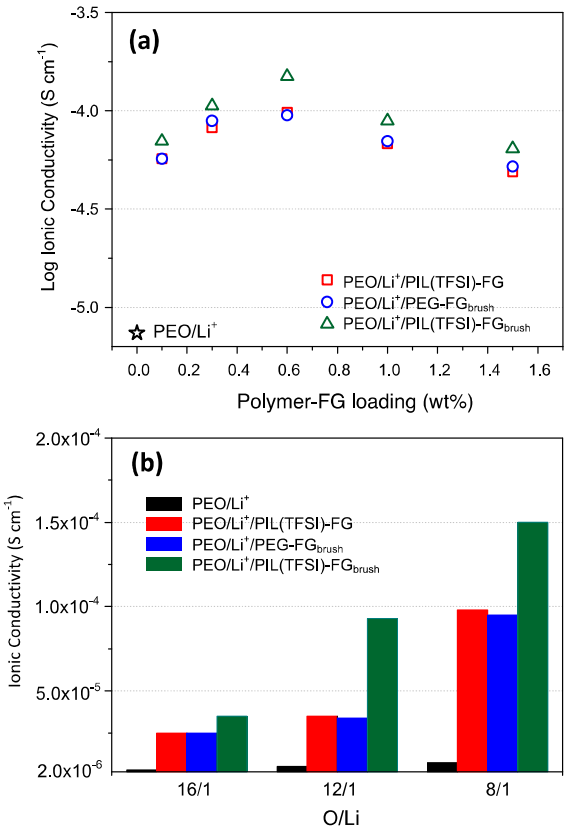

Figure 8. (a) Ion conductivity of PEO/Li^+ PEs at 60 ˚C with varying polymer-FG contents at an O/Li ratio of 8/1. (b) Ion conductivity of PEO/Li^+ PEs at 60 ˚C with 0.6 wt% polymer-FG contents at various salt concentrations.

The transference number measurements were performed to further characterize the PE for battery application. Both cationic and anionic motions contribute substantially to the total ionic transport number in liquid or PEs. Hence, the cationic (Li^+) transport number is an important parameter and has been evaluated by means of a combined a.c. and d.c. technique proposed by Evans et al.[39] Li ion transport values (Li^+) can be calculated from:

$$t_{Li^+} = \frac{I_S(\Delta V - R_0 I_0)}{I_0(\Delta V - R_S I_S)}$$

where I_0 and I_s are the initial and final currents; R_0 and R_s are the cell resistances before and after polarization. The values of t_{Li^+} evaluated at 60 ˚C for PEO and PEO/Li^+ PE with 0.6 wt% polymer-FG at an O/Li ratio of 8/1 are 0.18, 0.56, 0.52 and 0.68 for pure PEO/Li^+ PE, PEO/Li^+/PIL(TFSI)-FG, PEO/Li^+/PEG-FG_{brush} and PEO/Li^+/PIL(TFSI)-FG_{brush} CPEs, respectively. There is a remarkable enhancement (≥3-fold increase) in the Li^+ ion transport number by adding 0.6 wt% polymer-FG compared to the pure PEO/Li^+ PE, reaching a maximum value of 0.62 in the PEO/Li^+/PIL(TFSI)-FG_{brush} CPE. We speculate that the grafted PIL structure and the form of the RGO surface play an important role in the ion-surface interactions; the polymer segmental mobility also has an impact on ion transport in the CPEs.

Figure 9 shows schematically ion transfer through the PIL(TFSI)-FG_{brush} and polymer chains. The surface grafted PIL on these RGO sheets loosely binds anions (ClO_4^-) and frees cations, it also provides sites for conduction of loosely bound anions though the PE. Thus, Li^+ ions may find low-energy paths along the RGO sheets/polymer matrix interface. As a result, the PIL(TFSI)-FG_{brush} enhances the dissolvability of the Li salt and increases the free volume and segmental motion of the polymer matrix. Therefore, we can conclude that the introduction of the PIL(TFSI)-FG_{brush}, which has PIL brushes, not only offers ionic conducting channels along the interphase, also increases the number of mobile Li^+, increases amorphicity and re-dissociation of ion pairs, hence collectively contributing to the significant increase in ion transport through the PE.

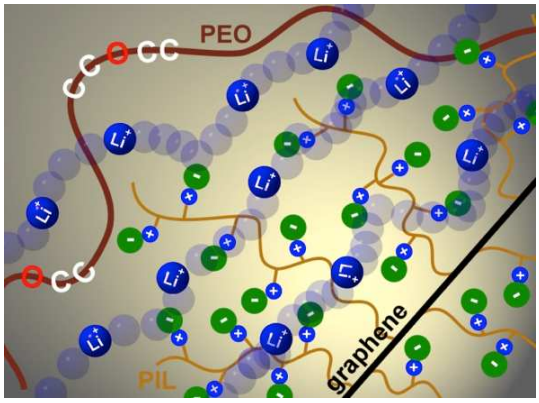

Figure 9. Illustration on Li ion transport mechanism in the PEO/Li^+/PIL(TFSI)-FG_{brush} CPE.

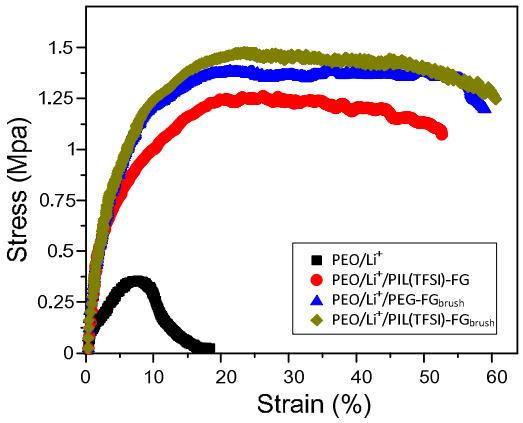

Figure 10. Stress-strain curves of PEO/Li^+ PE and PEO/Li^+/polymer-FG 0.6 wt% CPEs.

Mechanical Properties and Electrochemical Performance of PEO/Li^+ and PEO/Li^+/Polymer-FG CPEs

The mechanical properties of PEO/Li^+ PE and PEO/Li^+/polymer-FG CPEs are tested at an O/Li ratio of 16/1, because it is difficult to test the tensile strength of pure PEO/Li^+ PE at high salt concentration. The stress-strain curves for PEO/Li^+ PE and PEO/Li^+/CPEs with 0.6 wt% polymer-FG at an O/Li ratio of 16/1 are presented in **Figure 10**. The tensile strength of the pure PEO/Li^+ is 0.35±0.03 MPa. By comparing the CPEs with PIL(TFSI)-FG, PEG-FG_{brush} and PIL(TFSI)-FG_{brush}, it is found that the polymer-FGs with polymer brushes have much better reinforcing effect on the PEO/Li^+ PE than polymer-FG without polymer brushes. The PEO/Li^+/PIL(TFSI)-FG_{brush} 0.6 wt% CPE shows a tensile strength of 1.45±0.08 MPa indicating that the use of PIL(TFSI)-FG_{brush} lead to more than 300% improvement in the tensile strength of PEO/Li^+ PE. Moreover, a large enhancement of Young's modulus is observed when polymer-FG is introduced in PEO/Li^+, especially in the PEO/Li^+/PIL(TFSI)-FG_{brush} CPE. The enhancement in tensile strength of PEO/Li^+ is comparable or even slightly higher than CPEs with GO and CNT -clay nano-fillers at similar salt concentration.[21, 26] The significant reinforcing effects can be ascribed to the uniform dispersion of polymer-FG_{brush} in the PEO/Li^+ PE and good interfacial interaction due to polymer brushes on RGO surface.

The electrochemical stabilities of the PEO/Li^+/polymer-FG CPEs were evaluated using linear sweep voltammetry (LSV) with stainless steel/SPE/Li coin cell at 60 °C. The linear sweep voltammograms of PEO/Li^+ PE with polymer-FG (**Figure S6**) shows an abrupt rise in current at the voltage of 4.5~5 V (*vs.* Li/Li^+) corresponding to the electrochemical oxidative degradation of the PE. Similar electrochemical stability is observed in the PEO/Li^+/polymer-FG CPEs, which indicates that they are electrochemically stable within the operation voltage range of the $LiFePO_4$ cathode, and other 4V class cathode materials.

Figure 11 presents the discharge capacity of the Li/SPE/$LiFePO_4$ cell at 0.1 C and 60 °C during cycling. All the PEO/Li^+/polymer-FG CPEs having 0.6 wt% of polymer-FG at an O/Li ratio of 8/1 was chosen for the cell test because it

exhibited the highest ionic conductivity among the their CPEs. The discharge capacity of PEO/Li^+ PE is significantly improved from 120 mA h g^{-1} to 140, 143 and 156 mA h g^{-1} at first cycle by introducing PIL(TFSI)-FG, PEG-FG_{brush} and PIL(TFSI)-FG_{brush}, respectively (**Figure 11a**), which is ascribed to the faster Li transport of the PEO/Li^+/polymer-FG CPEs compared with the PEO/Li^+ PE.[43] After testing for 50 cycles, no obvious capacity loss is observed for all SPEs (**Figure 11b**), which is similar to other PEO-based SPE Li-ion battery systems.[44, 45] However, it is worth noting that the PEO/Li^+/PIL(TFSI)-FG_{brush} CPE displays a higher capacity which is about 30% enhancement compared to the pure PEO/Li^+ PE during 50 cycles. The high capacity and long-term cyclic stability of the PEO/Li^+/PIL(TFSI)-FG_{brush} CPE suggest that nano-fillers having a PIL and a polymer brush structure is a very effective and promising structural design to enhance the electrochemical performance of all-solid-state Li-ion batteries.

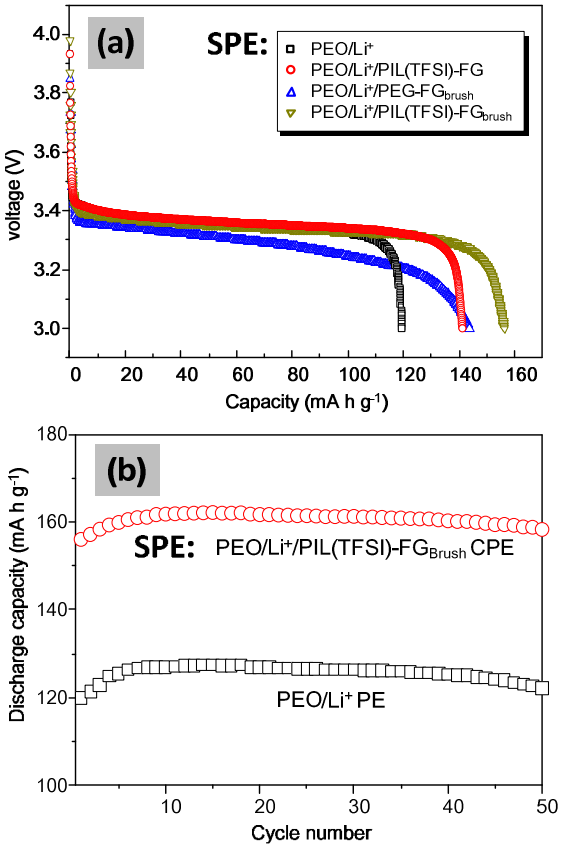

Figure 11. (a) Charge-discharge profiles of Li/SPE/$LiFePO_4$ cell at 60 °C; (b) Cyclic performance of Li/SPE/$LiFePO_4$ cell at 60 °C.

Conclusions

We have successfully prepared three types of polymer-FG with different structural design and tailored morphology incorporated into PEO/Li^+ PE to fabricate PEO/Li^+/polymer-FG CPEs. The Li-ion transfer conditions including dissociation of Li salt, amorphous content and segmental mobility in CPEs can be improved by the added polymer-FGs. In particular, optimal Li-ion transfer conditions and enhanced Li^+ transport numbers are achieved by incorporating the polymer-FG combining a PIL and a polymer brush structure [i.e., PIL(TFSI)-FG_{brush}]. The Li ion conductivity of PEO/Li^+ PE with PIL(TFSI)-FG_{brush} is enhanced by >2 orders of magnitude and ~20-fold at 30 and 60 ˚C with high salt loading (O/Li= 8/1), respectively. Furthermore, more than 300% increase in the tensile strength of the PEO/Li^+ PE are achieved with only 0.6 wt% PIL(TFSI)-FG_{brush} content at an O/Li ratio of 16/1. The PEO/Li^+/PIL(TFSI)-FG_{brush} CPE with high ionic conductivity exhibited high capacity and long-term cyclic stability when compared with pure PEO/Li^+ PE. The polymer functionalization strategy shown in this work paves the way to gaining a better understanding of the role of structural design and tailored morphology in polymer-FG, contributing to the development of high performance CPEs for all-solid-state Li-ion batteries.

Acknowledgements

The authors acknowledge the financial support of the National Natural Science Foundation of China (51210004 and 51433002).

Notes and references

1. F. Groce, F. Gerace, G. Dautzemberg, S. Passerini, G. B. Appetecchi and B. Scrosati, *Electrochim Acta*, 1994, 39, 2187-2194.
2. B. Oh and Y. R. Kim, *Solid State Ionics*, 1999, 124, 83-89.
3. L. Zhang, B. L. Chaloux, T. Saito, M. A. Hickner and J. L. Lutkenhaus, *Macromolecules*, 2011, 44, 9723-9730.
4. H. Zhang, S. Kulkarni and S. L. Wunder, *J Phys Chem B*, 2007, 111, 3583-3590.
5. I. E. Kelly, J. R. Owen and B. C. H. Steele, *J Power Sources*, 1985, 14, 13-21.
6. C. Capiglia, P. Mustarelli, E. Quartarone, C. Tomasi and A. Magistris, *Solid State Ionics*, 1999, 118, 73-79.
7. G. B. Appetecchi and S. Passerini, *Electrochim Acta*, 2000, 45, 2139-2145.
8. A. Manuel Stephan, K. Nahm, M. Anbu Kulandainathan, G. Ravi and J. Wilson, *Journal of Applied Electrochemistry*, 2006, 36, 1091-1097.
9. X. Q. Yang, H. S. Lee, L. Hanson, J. McBreen and Y. Okamoto, *J Power Sources*, 1995, 54, 198-204.
10. M. H. Sheldon, M. D. Glasse, R. J. Latham and R. G. Linford, *Solid State Ionics*, 1989, 34, 135-138.
11. D. T. Hallinan and N. P. Balsara, *Annu Rev Mater Res*, 2013, 43, 503-525.
12. M. C. Borghini, M. Mastragostino, S. Passerini and B. Scrosati, *J Electrochem Soc*, 1995, 142, 2118-2121.
13. F. Croce, L. Settimi and B. Scrosati, *Electrochem commun*, 2006, 8, 364-368.
14. F. Croce, R. Curini, A. Martinelli, L. Persi, F. Ronci, B. Scrosati and R. Caminiti, *J Phys Chem B*, 1999, 103, 10632-10638.
15. W. Wieczorek, J. R. Stevens and Z. Florjańczyk, *Solid State Ionics*, 1996, 85, 67-72.

16. B. Kumar and L. G. Scanlon, *Solid State Ionics*, 1999, 124, 239-254.
17. S. Kim, E.-J. Hwang, Y. Jung, M. Han and S.-J. Park, *Colloids and Surfaces A: Physicochemical and Engineering Aspects*, 2008, 313–314, 216-219.
18. H.-W. Chen, C.-Y. Chiu, H.-D. Wu, I. W. Shen and F.-C. Chang, *Polymer*, 2002, 43, 5011-5016.
19. G. Sandí, K. A. Carrado, H. Joachin, W. Lu and J. Prakash, *J Power Sources*, 2003, 119–121, 492-496.
20. A. Udomvech, T. Kerdcharoen and T. Osotchan, *Chem Phys Lett*, 2005, 406, 161-166.
21. C. Tang, K. Hackenberg, Q. Fu, P. M. Ajayan and H. Ardebili, *Nano Lett*, 2012, 12, 1152-1156.
22. Y.-S. Ye, C.-Y. Tseng, W.-C. Shen, J.-S. Wang, K.-J. Chen, M.-Y. Cheng, J. Rick, Y.-J. Huang, F.-C. Chang and B.-J. Hwang, *Journal of Materials Chemistry*, 2011, 21, 10448-10453.
23. C.-Y. Tseng, Y.-S. Ye, M.-Y. Cheng, K.-Y. Kao, W.-C. Shen, J. Rick, J.-C. Chen and B.-J. Hwang, *Advanced Energy Materials*, 2011, 1, 1220-1224.
24. B. G. Choi, J. Hong, Y. C. Park, D. H. Jung, W. H. Hong, P. T. Hammond and H. Park, *ACS Nano*, 2011, 5, 5167-5174.
25. Y.-S. Ye, M.-Y. Cheng, X.-L. Xie, J. Rick, Y.-J. Huang, F.-C. Chang and B.-J. Hwang, *J Power Sources*, 2013, 239, 424-432.
26. M. Yuan, J. Erdman, C. Tang and H. Ardebili, *RSC Adv*, 2014, 4, 59637-59642.
27. J. Shim, D.-G. Kim, H. J. Kim, J. H. Lee, J.-H. Baik and J.-C. Lee, *J Mater Chem A*, 2014, 2, 13873-13883.
28. H. Wang, S.-G. Bi, Y.-S. Ye, Y. Xue, X.-L. Xie and Y.-W. Mai, *Nanoscale*, 2015, 7, 3548-3557.
29. G. Sakellariou, D. Priftis and D. Baskaran, *Chem Soc Rev*, 2013.
30. R. K. Layek and A. K. Nandi, *Polymer*, 2013, 54, 5087-5103.
31. Y. S. Ye, H. Wang, S. G. Bi, Y. Xue, Z. G. Xue, Y. G. Liao, X. P. Zhou, X. L. Xie and Y. W. Mai, *Carbon*, 2015, 86, 86-97.
32. Y. Liu, J. Y. Lee and L. Hong, *J Power Sources*, 2004, 129, 303-311.
33. L. Kan, Z. Xu and C. Gao, *Macromolecules*, 2010, 44, 444-452.
34. D. Mecerreyes, *Prog Polym Sci*, 2011, 36, 1629-1648.
35. Y.-S. Ye, J. Rick and B.-J. Hwang, *J Mater Chem A*, 2013, 1, 2719-2743.
36. Y.-S. Ye, Y.-N. Chen, J.-S. Wang, J. Rick, Y.-J. Huang, F.-C. Chang and B.-J. Hwang, *Chem Mater*, 2012, 24, 2987-2997.
37. Y.-S. Ye, W.-C. Shen, C.-Y. Tseng, J. Rick, Y.-J. Huang, F.-C. Chang and B.-J. Hwang, *Chem Commun*, 2011, 47, 10656-10658.
38. M. Li, B. Yang, L. Wang, Y. Zhang, Z. Zhang, S. Fang and Z. Zhang, *J Memb Sci*, 2013, 447, 222-227.
39. J. Evans, C. A. Vincent and P. G. Bruce, *Polymer*, 1987, 28, 2324-2328.
40. G. L. Hwang, Y. T. Shieh and K. C. Hwang, *Adv Funct Mater*, 2004, 14, 487-491.
41. P. G. Bruce and C. A. Vincent, *Journal of the Chemical Society, Faraday Transactions*, 1993, 89, 3187-3203.
42. W. H. Meyer, *Adv Mater*, 1998, 10, 439-448.
43. H.-J. Ha, E.-H. Kil, Y. H. Kwon, J. Y. Kim, C. K. Lee and S.-Y. Lee, *Energy & Environmental Science*, 2012, 5, 6491-6499.
44. M. Nakayama, S. Wada, S. Kuroki and M. Nogami, *Energy & Environmental Science*, 2010, 3, 1995-2002.
45. Y. Masuda, M. Nakayama and M. Wakihara, *Solid State Ionics*, 2007, 178, 981-986.